Research Square

Preprints are preliminary reports that have not undergone peer review.
They should not be considered conclusive, used to inform clinical practice,
or referenced by the media as validated information.

Identification of Triaptosis-Related Prognostic Genes and Construction of a Predictive Model in Breast Cancer

Tianyi Zhao
The First Affiliated Hospital of Shenzhen University
Haiying Liu
The First Affiliated Hospital of Shenzhen University
Xianlong Yang
The First Affiliated Hospital of Shenzhen University
Chuhan Luoliu
The First Affiliated Hospital of Shenzhen University
Can Zhang
Shenzhen Longgang District Maternity & Child Healthcare Hospital
Ran Liu
Shenzhen University, Shenzhen University Medical School
Jiawen Zhao
Shenzhen University, Shenzhen University Medical School
Guowen Liu
liugw8318@163.com

The First Affiliated Hospital of Shenzhen University

Research Article

Keywords: Breast cancer, Triaptosis, Prognostic genes, Prognostic model, Immune infiltration analysis, Drug sensitivity

Posted Date: June 29th, 2026

DOI: https://doi.org/10.21203/rs.3.rs-9716459/v1

License: This work is licensed under a Creative Commons Attribution 4.0 International License.
Read Full License

Additional Declarations: No competing interests reported.

Identification of Triaptosis-Related Prognostic Genes and Construction of a Predictive Model in Breast Cancer

Tianyi Zhao[1,2], Haiying Liu[1,2], Xianlong Yang[1,2], Chuhan Luoliu [1,2], Can Zhang[3], Ran Liu[2], Jiawen Zhao[2], Guowen Liu[1*]

[1]Shenzhen Second People's Hospital, The First Affiliated Hospital of Shenzhen University, Department of Thyroid and Breast Surgery, Shenzhen, 518035, Guangdong, China

[2]Shenzhen University, Shenzhen University Medical School, Shenzhen, 518060, Guangdong, China

[3]Shenzhen Longgang District Maternity & Child Healthcare Hospital, Department of Thyroid and Breast Surgery, Shenzhen, 518172, Guangdong, China

*** Correspondence:**
Guowen Liu
liugw8318@163.com

Keywords: Breast cancer, Triaptosis, Prognostic genes, Prognostic model, Immune infiltration analysis, Drug sensitivity.

Abstract

Background: Breast cancer (BC) is one of the most common malignancies in women worldwide. Triaptosis, a recently proposed oxidative cell death characterized by endosomal dysfunction, has an unclear role in BC.

Methods: We used BC transcriptome data and triaptosis-related genes to identify module genes by WGCNA. Candidate genes were intersected with differentially expressed genes (DEGs). Prognostic genes were screened by univariate Cox and LASSO regression. Functional enrichment, drug prediction, immune infiltration, immune checkpoint, pathway, and drug sensitivity analyses were performed. A nomogram was constructed, and RT-qPCR was used for validation.

Results: We identified 3,396 triaptosis-related module genes and 578 candidate genes. Three prognostic genes, BNIP3L, KLHDC1, and PRDX3, were selected. These genes were enriched in multiple pathways, including oxidative phosphorylation, and were linked to potential targeted drugs. The nomogram combining risk score and tumor size showed good predictive performance. MDSCs were significantly associated with the three genes. Immune checkpoint molecules and several metabolic pathways differed between risk groups. In addition, 64 drugs showed significant sensitivity differences. RT-qPCR confirmed lower expression of BNIP3L and PRDX3 in BC tissues ($p < 0.05$), while the expression of KLHDC1 also decreased, but without statistical significance.

Conclusion: This study identified three triaptosis-related prognostic genes in BC, providing new insights into the mechanisms of triaptosis, novel risk stratification markers, and personalized therapeutic targets.

Clinical trial number: not applicable.

1 Introduction

Breast cancer is the most frequent cancer in women, and the leading cause of death from cancer among women worldwide. BC accounts for about 30% of all cancers of women in the world and has a mortality-to-incidence ratio of 15% [1, 2]. By January 1, 2025, there are an estimated 4.3 million women diagnosed with invasive BC in the United States, and this number is predicted to increase to 5.3 million by 2035 [3]. Therefore, BC has become a major public health issue that threatens women's lives. BC exhibits substantial molecular and clinical heterogeneity. The prevailing clinical subclassification scheme hinges on the immunohistochemical detection of three critical hormone and growth factor receptors—estrogen receptor (ER), progesterone receptor (PR), and human epidermal growth factor receptor 2 (HER2)—yielding four principal subtypes: Luminal A, Luminal B, HER2-positive, and triple-negative breast cancer (TNBC) [4]. These molecular subtypes significantly differ in their biological behavior, response to treatment, and clinical outcome, and TNBC has the worst clinical outcome in the absence of effective therapeutic targeting [5]. Despite the development of a multidisciplinary, comprehensive treatment paradigm based on surgery, radiotherapy, chemotherapy, endocrine therapy, targeted therapy, and immunotherapy [6], challenges such as tumor recurrence, distant metastasis, and therapeutic resistance remain huge clinical problems [7]. Thus, understanding the core molecular pathways of BC occurrence and development, and discovering new prognostic biomarkers and therapeutic targets is imperative to obtain precise prediction and therapy, and ultimately enhance patients' survival, especially for resistant subtypes.

Programmed cell death (PCD) is an important physiological process for tissue homeostasis, and its dysregulation is associated with tumorigenesis and development [8]. Besides classical apoptosis and ferroptosis, a newly identified oxidative cell death, "triaptosis", has recently been discovered [9]. Triaptosis is provoked by pro-oxidants such as the vitamin K precursor menadione sodium bisulfite (MSB), and its main mechanism is the oxidation of a key kinase, type III phosphatidylinositol 3-kinase catalytic subunit (VPS34), leading to the depletion of phosphatidylinositol 3-phosphate (PI (3) P), an essential signaling lipid in the intracellular membrane system. PI (3) P depletion results in the malfunction of endosomes, and their identity is abrogated and eventually accumulated excessively in the cell, triggering cell death [10]. Given that this lethal process is initiated by pro-oxidant stress, cellular machineries that govern redox homeostasis and endosomal integrity are likely critical gatekeepers against triaptosis. The therapeutic relevance of this pathway has been demonstrated in prostate cancer models, where MSB-induced triaptosis exerted a persistent antitumor effect [11]. However, whether triaptosisexists in BC, the regulatory network, and its relationship with tumor development and patient's prognosis are unclear. Investigation into the correlation of triaptosis with BC will not only aid in discovering novel tumor biological mechanisms but may also provide innovative solutions to existing treatment resistance.

This study systematically investigates the clinical significance and potential molecular mechanisms of triaptosis in BC. By integrating bioinformatics analysis, we identified prognostic genes closely associated with the triaptosis process, constructed a prognostic model, and conducted functional enrichment profiling and quantified tumor immune cell infiltration, and drug sensitivity prediction. This work elucidates the potential pathogenic mechanisms of BC from a novel perspective and provides potential molecular targets for future tailored therapeutic strategies.

2 Materials and methods

2.1 Data sources

The dataset GSE42568 was downloaded from the Gene Expression Omnibus (GEO) database (https://www.ncbi.nlm.nih.gov/geo/) (sequencing platform: GPL570; sequencing type: array; download date: 2025-09-20), which includes 104 BC patient samples (disease group) and 17 normal samples (control group). All BC patient samples had survival information. The dataset contained clinical characteristics such as age, estrogen receptor (ER) status, clinical stage, lymph node status, and tumor size, and was used as the training set [12]. Subsequently, the dataset GSE20685 was downloaded from the GEO database (https://www.ncbi.nlm.nih.gov/geo/) (sequencing platform: GPL570; sequencing type: array; download date: 2025-09-20), which includes 327 BC patient samples, all with survival information, and was used as the validation set [13]. Additionally, 21 triaptosis-related genes were sourced from the referenced literature [14] (**Table S1**).

2.2 WGCNA

To evaluate whether triaptosis-related genes played a role in BC, the R package "GSVA" (v 1.53.28) [15] was utilized to score triaptosis-related genes in the GSE42568 cohort. The Wilcoxon rank-sum test was subsequently employed to evaluate differences in scores between the disease and control cohorts ($p < 0.05$). Subsequently, the optimal cutoff for dividing the dataset was determined by the R package "survminer" (v 0.4.9) [16]. Based on this cut-off point, BC patients

were stratified into high-score and low-score groups using the R package "survival" (v 3.7-0)[17], and survival analysis was performed ($p < 0.05$). To better identify the genes linked to directional genes, WGCNA was performed on the disease samples from the GSE42568 dataset viathe R package "WGCNA" (v 1.73) [18], with GSVA scores as the trait. First, the goodSamplesGenesfunction was used to remove unqualified genes and samples. Sample hierarchical clustering via the hclustfunction was performed to determineand exclude outlier samples. Next, soft threshold screening was carried out. The optimal soft threshold (β) was determined based on the scale-free topology criterion when the scale-free fit index R^2 approached 0.9 and the mean connectivity stabilized. The minimum module size was set to 50. The module merge threshold was set to 0.25. This was done to obtain co-expression modules. Key modules were determined by computing the Pearson correlation coefficients (cor) between module eigengenes and the trait, with screening criteria set at $|cor| > 0.3$ and $p < 0.05$. For genes within the key modules, module membership (MM) and gene significance (GS) were computed. Scatter plots were used to visualize the correlation distribution between MM and GS, aiming to identify core genes exhibiting both high module connectivity and high trait relevance. These genes were designated as triaptosis-associated module genes and carried forward for downstream analysis.

2.3 Differential expression analysis

To detect DEGs between BC patient samples and normal samples, differential analysis was implemented using the R package "DESeq2" (v 1.40.2) [19] on the GSE42568 cohort. (adjusted p (adj.p) < 0.05,$|\log_2$ Fold Change (FC)$| > 1$). Subsequently, the R packages "ggplot2" (v 3.5.1) [20]and "ComplexHeatmap" (v 2.16.0) [21] were utilized to visualization.

2.4 Candidate genes screening and functional analysis

The DEGs were crossed with the genes in the triaptosis-related module to identify candidates, and the results of this intersection were shown with the R package "ggvenn" (v 0.1.10) [22]. Functional enrichment analyses were conducted for GO terms and KEGG pathways using the R package "clusterProfiler" (v 4.15.0) [18] (adj.p < 0.05). Moreover, a PPI network encompassing the candidate genes was generated withthe STRING database (https://string-db.org)(confidence score >0.40).

2.5 Identification of prognostic genes

In BC patient samples with survival information from the GSE42568 cohort, univariate Cox regression analysis was implemented on the candidate genes using the R package "survival" (v 3.7-0) [17] ($HR \neq 1$, $p < 0.05$), and a forest plotwere plotted viathe R package "forestplot" (v 3.1.5) [23]. To ensure the validity of the univariate analysis results, the PH assumption was then tested viathe R package "survival" (v 3.7-0) [17] ($p > 0.05$). Subsequently, for genes which passed the PH assumption test, LASSO analysis was implemented using the R package "glmnet" (v 4.1-8) [24]. This method shrunk the coefficients of genes with weaker associations to zero while retaining those with stronger associations to the disease outcome. The optimal model was determined through 10-fold cross-validation, and prognostic genes were determined based on the $\log\lambda_{min}$value corresponding to the minimum error rate of the model.

2.6 GSEA of prognostic genes

The KEGG gene set (c2.cp.kegg.v7.5.1.symbols.gmt) from the C2: Curated Gene Sets collection was retrieved via the R package "msigdbr" (v 7.5.1) [25] as the reference gene set. Subsequently, the R package "psych" (v 2.2.9) [26] was] was employed to compute the Spearman correlation coefficients between each prognostic gene and all genes, with genes arranged in descending order according to regression coefficients, yielding a prioritized gene list for each prognostic signature. Then, GSEA was implemented via the R package "clusterProfiler" (v 4.15.0) [18] ($|NES| > 1$, FDR < 0.25, $p < 0.05$).

2.7 Drug prediction for prognostic genes

To explore potential therapeutic agents for BC, drug compound predictions were performed with the DsigDB(https://dsigdb.tanlab.org/DSigDBv1.0/). The drug-gene interaction derived from the prognostic gene set was rendered using Cytoscape (v 3.10.3) [27].

2.8 Prognostic models establishment and validation

In the GSE42568 cohort, the risk score was computed using the risk model formula that had been defined beforehand. Patients were separated into the high-risk group (HRG) and low-risk group (LRG) with the optimal cutoff derived from

survival analysis, and a corresponding risk distribution plot was constructed. The R package "survival" (v 3.7-0) [17] was applied to plot Kaplan-Meier (K-M) survival curves and assess survival differences between the HRG and LRG. At 3-, 5- and 7-year time points [28, 29], time-dependent ROC curves were created using the R package "timeROC" (v 0.4) [28] (AUC > 0.6). The same analytical procedures were applied to the GSE20685 cohort to validate the risk model. The risk score was computed as follows:

$$risk\ score = \sum_{(i=1)}^{n} coef(i) \times expr(i)$$

Where coefrepresented the coefficient derived from LASSO analysis, and expr denoted the gene expression level. The specific coefvalues were presented in **Table S2**.

2.9 Independent prognostic analysis

Clinical characteristics (including age, ER status, clinical stage, lymph node status, and tumor size) and risk scores from BC patients in the GSE42568 cohort were integrated. Univariate Cox proportional hazards regression was implemented using the R package "survival" (v 3.7-0) [17], with variables screened based on a HR ≠ 1 and $p < 0.05$, followed by verification of the PH assumption ($p > 0.05$). Covariates exhibiting statistical significance in univariate Cox regression were advanced to multivariate Cox proportional hazards modeling (HR ≠ 1, $p < 0.05$, PH $p > 0.05$). A nomogram was established using the R package "rms" (v 6.8-1) [29], followed by calibration plots for 3-, 5- and 7-year survival probabilities generated. Moreover, time-dependent ROC curves for the nomogram were constructed at 3-, 5- and 7-year time points via the R package "timeROC" (v 0.4) [28] (AUC > 0.7).

2.10 Immune infiltration analysis

Based on all BC samples with survival data in the GSE42568 cohort, the relative abundance of 28 immune cell subsets was calculated via ssGSEA. The Wilcoxon rank-sum test was applied to assess statistically significant variations in immune cell infiltration levels between the HRG and LRG ($p < 0.05$). To examine the interrelationships among immune cell populations exhibiting differential infiltration, Spearman correlation coefficients were computed via the R package "psych"(v 2.2.9) [26] ($|cor| > 0.3$, $p < 0.05$). Additionally, associations between immune cell types showing differential infiltration and prognostic genes were assessed via correlation analysis ($|cor| > 0.3$, $p < 0.05$), followed by a heatmap depicted via the R package "corrplot" (v 0.95) [30].

2.11 Immune checkpoint analysis

A list of 47 immune checkpoint-related genes was obtained from relevant literature [31]. The Wilcoxon rank-sum test was applied to assess the immune checkpoint gene expression levels of the HRG and LRG ($p < 0.05$). Spearman's rank correlation method was implemented on immune checkpoint genes that showed significant differential expression, viathe R package "psych" (v 2.2.9) [26]to evaluate their associations with the prognostic genes ($|cor| > 0.3$, $p < 0.05$).

2.12 GSEA of the HRG and LRG

KEGG pathway gene sets (c2.cp.kegg.v7.5.1.symbols.gmt) were obtained from the MSigDB2 collection via the R package "msigdbr" (v 7.5.1) [25] and used as the reference. Differential expression analysis was implemented using the R package "DESeq2" (v 1.40.2) [19]. Genes were ranked by log_2FC values to generate a sorted gene list, which was subsequently subjected to GSEA via the R package "clusterProfiler" (v 4.15.0) [18] ($|NES| > 1$, adj.$p < 0.05$).

2.13 Drug sensitivity analysis

Based on BC samples with survival information from the GSE42568 cohort, the R package "pRRophetic" (v 0.5) [32] was applied to access built-in drug sensitivity data and compute the IC50 values. A higher IC50 value indicates poorer drug efficacy. IC50 values were compared between the HRG and LRG through the Wilcoxon rank-sum test ($p < 0.05$).

2.14 Expression analysis of prognostic genes

Further analysis was implemented to observe prognostic gene expression through RT-qPCR. Samples of BC tumour tissue and paracancerous tissue were obtained from five BC patients at Shenzhen Second People's Hospital. This study was given approval by the Clinical Research Ethics Committee of Shenzhen Second People's Hospital. All patients had

signed an informed consent form. Total RNA was extracted separately from each sample via TRIzol (Ambion, Austin, USA). The process of reverse transcription of total RNA to cDNA was carried out using a SureScript-First-Strand-cDNA-Synthesis-Kit (Servicebio, Wuhan, China), following the instructions provided by the manufacturer. We performed RT-qPCR using the 2xUniversal Blue SYBR Green qPCR Master Mix (Servicebio, Wuhan, China). The primer sequences for PCR are shown in **Table S3**. The $2^{-\Delta\Delta Ct}$method [33] was applied to estimate prognostic gene expression, and the resultant data were statistically analyzed and plotted by GraphpadPrism (v 8.0) software [34].

2.15 Statistical analysis

R (v 4.3.3) was applied to conduct the bioinformatics analysis. Differences between the two groups were assessed using the Wilcoxon test ($p < 0.05$).

3 Results

3.1 Identification of triaptosis-related module genes by WGCNA

The triaptosis-related genes score showed a significant difference between the disease and control groups ($p < 0.05$) (**Figure 1A**). Using the optimal cutoff value of 0.058, patients were stratified into high-score and low-score groups. K–M survival analysis showed a statistical difference in survival between the two risk groups ($p = 0.033$) (**Figure 1B**), indicating a strong association between triaptosisand the risk of mortality in BC patients. Sample clustering analysis demonstrated no outliers in the training set, confirming that all samples met the requirements for subsequent WGCNA (**Figure 1C**). Asoft threshold β of 7 was determined, under which the network exhibited scale-free topology characteristics (scale-free $R^2 \approx 0.9$, mean connectivity approaching 0) (**Figure 1D**). With a soft-thresholding power of 7, a minimum module size of 50 genes, and a module fusion cutoff of 0.25, the WGCNA analysis identified 13 robust co-expression modules. The gray module, which contained genes with weak correlations, was excluded from further analysis (**Figure 1E**). The turquoise module exhibitedthe strongestcorrelated with the triaptosisscore (cor= 0.56, $p < 0.05$) and contained 3,396 genes (**Figure 1F, Table S4**). Further analysis demonstrated a significant correlation between GS and MM in this module, and all 3,396 genes were selected as triaptosis-related module genes (**Figure 1G**). This study successfully identified the core gene module most closely associated with triaptosis, providing critical targets for elucidating its functional mechanisms in BC.

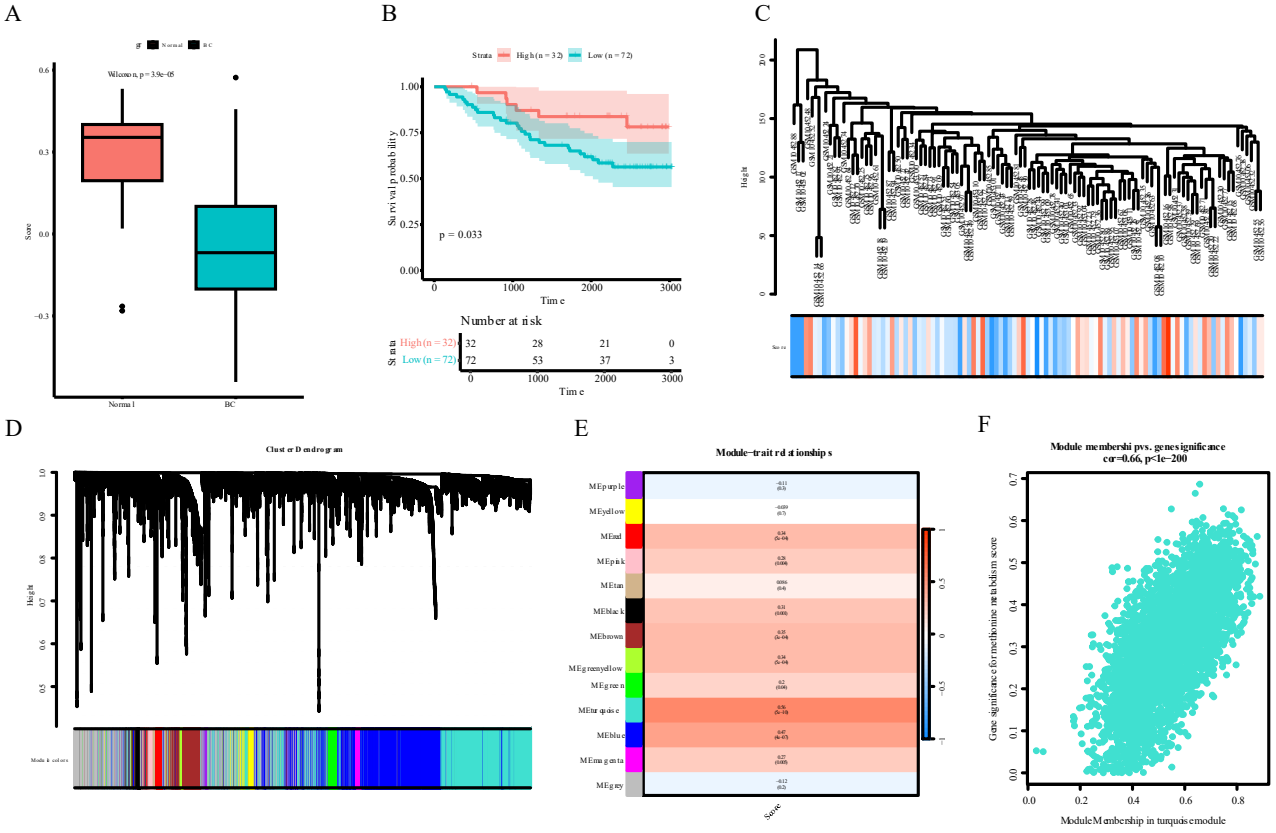


Fig. 1 Identification of triaptosis-related module genes by WGCNA (A) Differences in triaptosis-related gene scores between BC samples and normal samples; (B) Survival curves of patient groups stratified by triaptosis-related gene scores; (C) Sample clustering dendrogram; (D) Analysis of network topology; (E) Gene clustering dendrogram and module assignment; (F) Heatmap of module-trait relationships; (G) Gene clustering dendrogram and identified gene modules.

3.2 Identification of candidate genes and functional analysis in BC

Through differential expression gene analysis of BC samples compared to normal samples, 3,084 DEGs were identified, comprising 1,745 upregulated and 1,339 downregulated genes (**Figure 2A-B, Table S5**). Intersection with 3,396 triaptosis-related module genes yielded 578 overlapping genes, accounting for 9.8% of the total, which were selected as candidate genes for subsequent studies (**Figure 2C, Table S6**). GO analysis revealed 44 significantly enriched terms, comprising 37 biological processes (BPs) and 7 cellular components (CCs) (adj.p < 0.05) (**Figure 2D, Table S7**). In BPs, the candidate genes were primarily involved in endosomal transport, cytosolic transport, and the tricarboxylic acid (TCA) cycle; in CCs, they were primarily associated with the TCA cycle enzyme complex, mitochondrial matrix, and early endosomal compartments. KEGG analysis demonstrated that the candidate genes were shown to be highly enriched in six metabolism-related pathways, with the most prominent being the carbon metabolism, TCA cycle, and pyruvate metabolism (**Figure 2E**). PPI network analysis showed that 445 candidate genes made up a network with 1339 interactions and identified tightly interconnected modules around the core genes TP53, PTEN, SIRT1, and PDHB **(Figure 2F)**. These findings indicated that the candidate genes primarily participated in carbon metabolism, TCA cycle, and pyruvate metabolism, and the core regulatory genes TP53, PTEN, and SIRT1, which are an important theoretical basis for further study of their functions in the progression and development of BC.

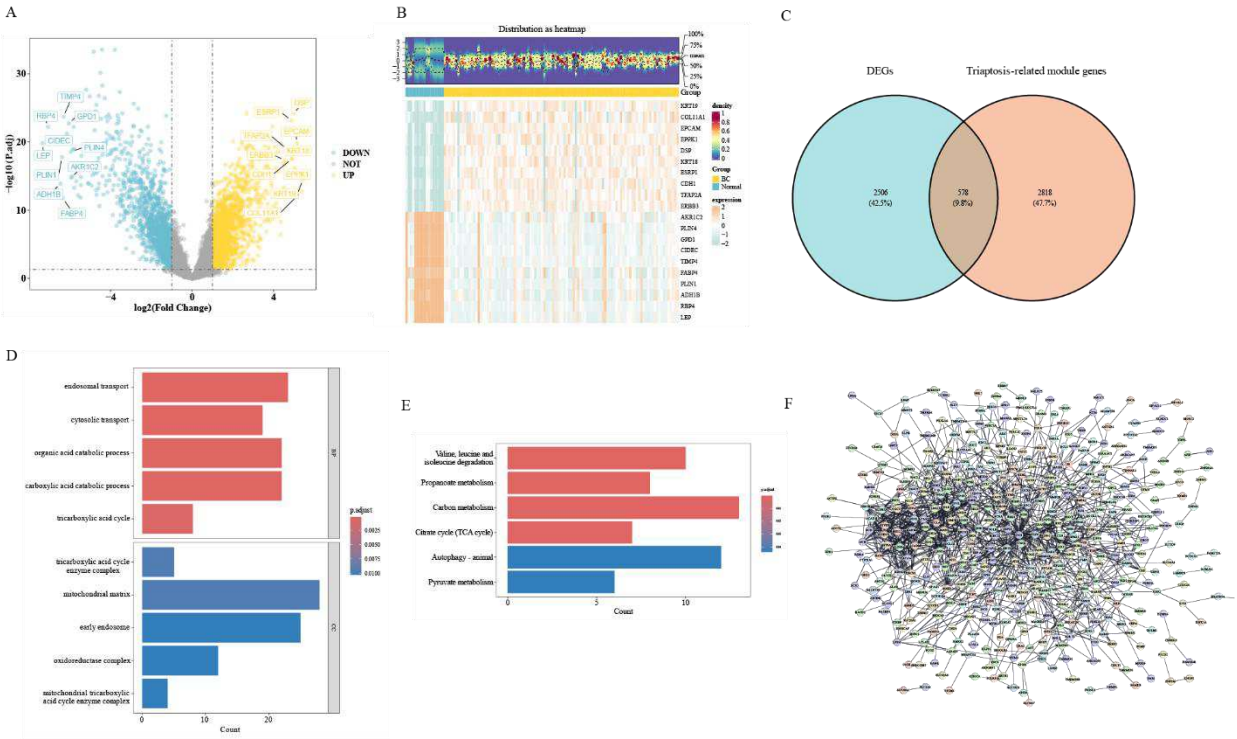


Fig. 2 Identification of candidate genes and functional analysis (A) Volcano plot of DEGs; (B) Heatmap of DEGs; (C) Venn diagram of candidate genes; (D) GO analysis of candidate genes; (E) KEGG analysis of candidate genes; (F) PPI network of candidate genes.

3.3 Identification of three prognostic genes through univariate Cox and LASSO regression analyses

Univariate Cox regression analysis uncovered 268 genes significantly linked to BC prognosis (HR ≠ 1 and p < 0.05) (**Table S8**). Among these, 233 genes were protective (HR < 1), with the top five genes exhibiting the lowest HR being ALG9, BNIP3L, ETFDH, LLPH, and KIF3A; 35 genes were risk genes (HR > 1), with the top five genes showing the highest HR being MORC2, YIPF2, MAP7D3, LSG1, and PYCR1 (**Figure 3A**). The PH assumption test confirmed 265

genes met the criteria ($p > 0.05$) (**Table S9**). Further LASSO regression analysis, with the minimum model error as the criterion, ultimately identified three prognostic genes at $\log\lambda_{min} = -1.64$: BNIP3L, KLHDC1, and PRDX3 (**Figure 3B-C**).

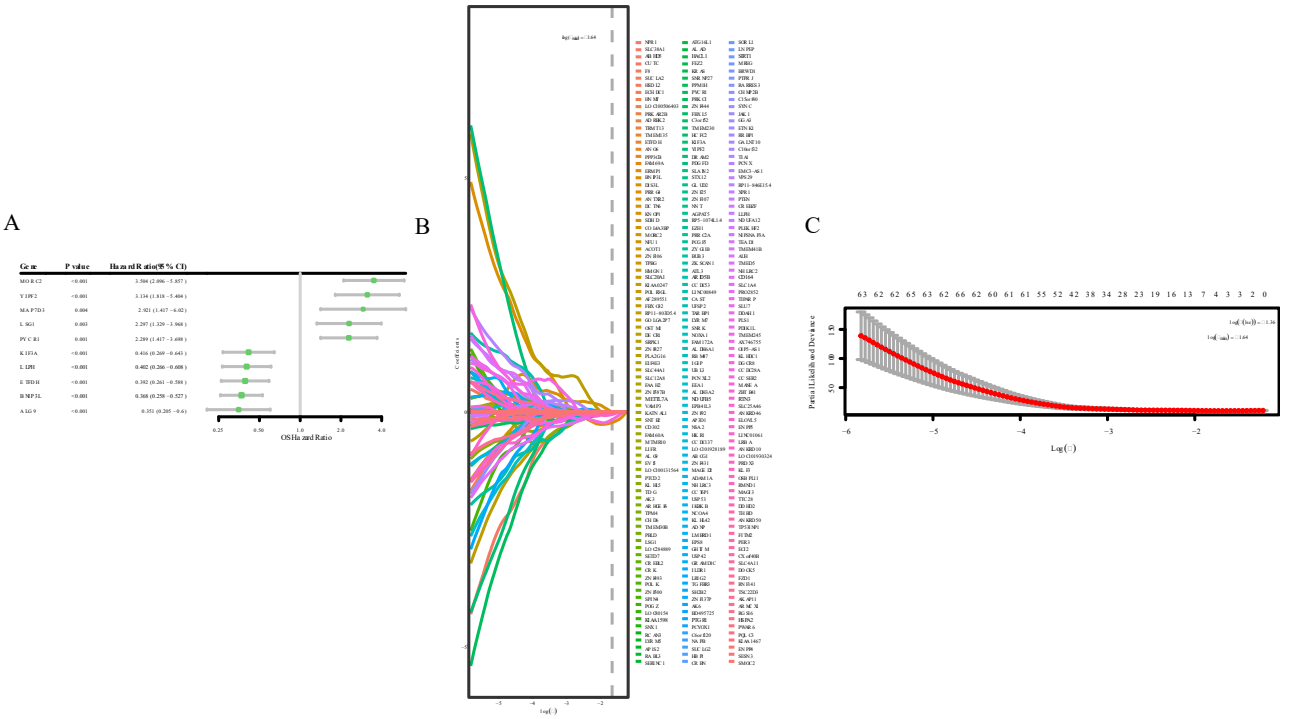


Fig. 3 Identification of prognostic genes (A) Forest plot of the univariable Cox regression analysis; (B) Coefficient profile plot of the LASSO regression analysis; (C) Cross-validation curve for tuning parameter selection in the LASSO regression.

3.4 Functional characterization of three prognostic genes revealed their pathway enrichment and potential targeted therapeutics.

Pathway enrichment of the three prognostic genes identified that BNIP3L was significantly enriched in 49 pathways **(Table S10, Figure 4A),** including pathways related to fatty acid metabolism, oxidative phosphorylation, and cell cycle regulation. KLHDC1 was enriched in 40 pathways **(Table S11, Figure 4B)**, mainly related to DNA replication, leucine and isoleucine degradation, valine, and propanoate metabolism. PRDX3 was enriched in 47 pathways **(Table S12, Figure 4C)**, significantly correlated with oxidative phosphorylation, citrate cycle (TCA cycle) and ubiquitin-mediated proteolysis. These pathway enrichment patterns of the three core prognostic genes collectively defined their distinct metabolic and functional role in BC pathogenesis. Then, through drug prediction analysis, 95 possible drugs targeting BNIP3L, 2 possible drugs targeting KLHDC1 and 28 possible drugs targeting PRDX3, such as tamoxifen **(Table S13, Figure 4D)**, were identified. These results demonstrated the important role of the three core prognostic genes BNIP3L, KLHDC1 and PRDX3 in metabolic regulation, signal transduction and neurodegeneration-related pathways. More than that, several possible therapeutic targeted drugs were identified.

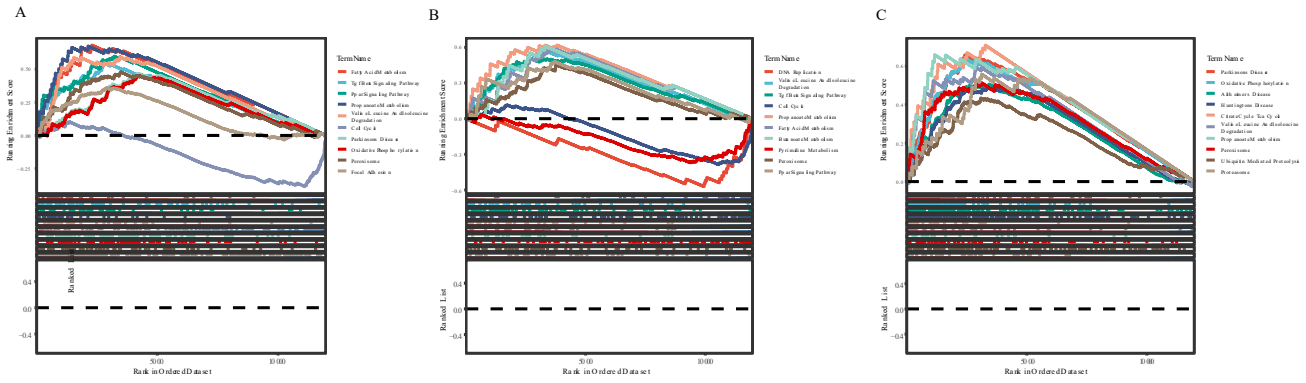


Fig. 4 Functional analysis of the prognostic genes (A-C) GSEA results for the prognostic genes BNIP3L, KLHDC1, and PRDX3, respectively; (D) Drug-gene interaction network of the prognostic genes.

3.5 Prognostic model based on three-gene signature demonstrates robust predictive performance

Based on the optimal risk-score cutoff of −3.5 determined by the prognostic gene signature, patients in the training cohort were separated into two subgroups: HRG (38 cases) and LRG (66 cases). **(Table S14)**. We found the number of deaths significantly increased in the HRG versus that in the LRG **(Figure 5A)**. K–M survival analysis showed a highly significant separation in overall survival between the HRG and LRG ($p < 0.0001$), with the HRG exhibiting markedly worse clinical outcomes **(Figure 5B)**. AUC values were 0.77, 0.83 and 0.89 at 3, 5, and 7 years, respectively **(Figure 5C)**, indicating that these three prognostic genes were clinically efficient in predicting patient survival status and the risk model showed good performance. The model also showed a good discriminative ability in a validation set. Patients were dichotomized into the HRG(252cases) and the LRG(75cases) cohorts with the optimal risk-score threshold of −5.23. **(Table S15)**. There were significantly more deaths in the HRG than in the LRG **(Figure 5D)**. The log-rank test confirmed a statistically significant variation in survival distribution between the HRG and LRG ($p < 0.0001$) **(Figure 5E)**, with markedly reduced survival probability observed in the HRG. Additionally, the AUC values at 3-, 5- and 7-year all exceeded 0.6, confirming the robustness of the prognostic model in the GSE20685 cohort (**Figure 5F**). This model successfully achieved precise risk stratification of BC patients, providing a reliable tool for clinical prognosis assessment.

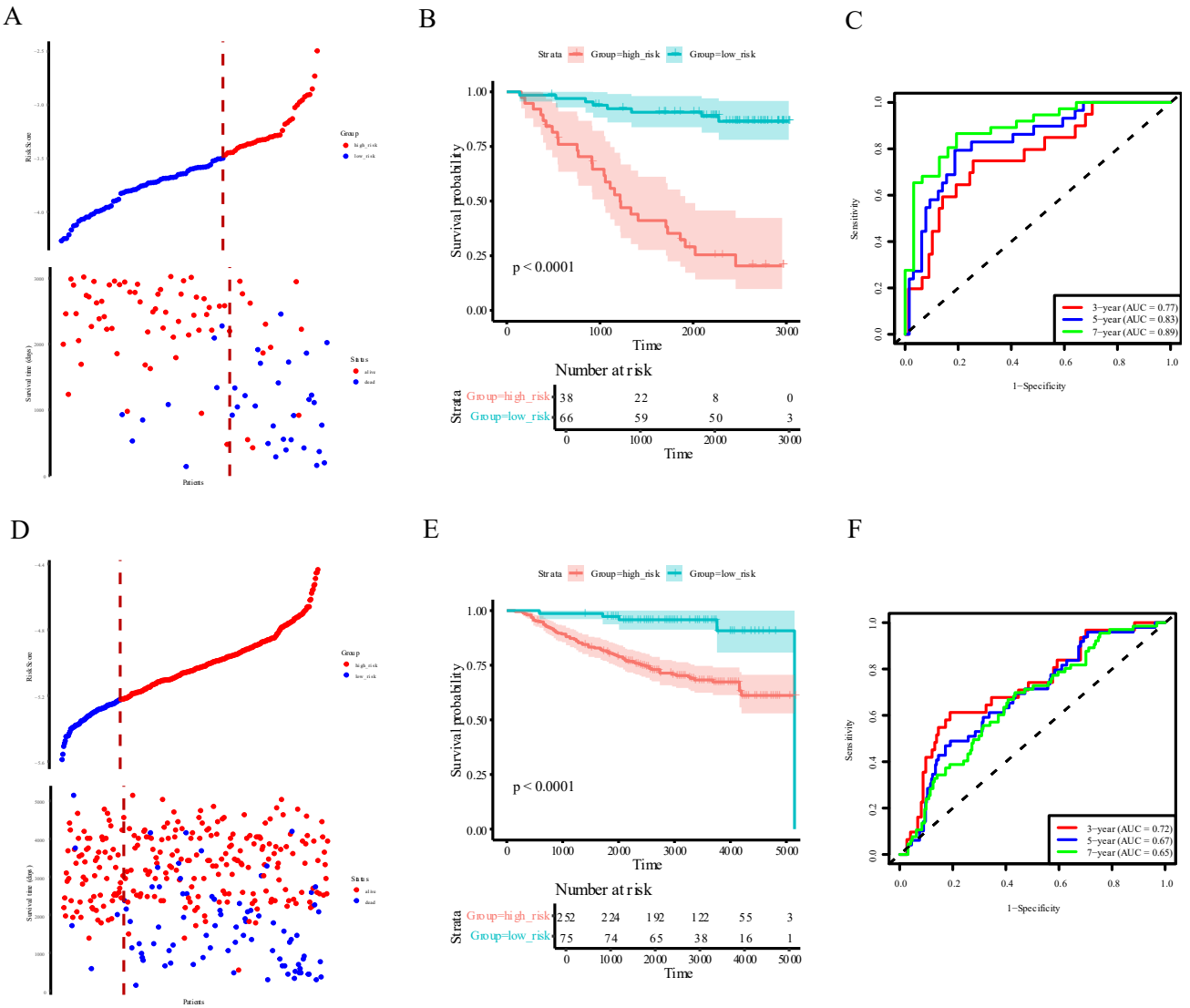


Fig. 5 Construction and validation of the prognostic model (A) Distribution of survival time and status for patients in the training set; (B) Kaplan-Meier survival curves in the training set; (C) ROC curve in the training set; (D) Distribution

of survival time and status for patients in the validation set; (E) Kaplan-Meier survival curves in the validation set; (F) ROC curve in the validation set.

3.6 Development and verification of prognostic nomogram incorporating tumor size and risk score for survival prediction in BC

Univariate Cox proportional hazards regression identified the tumor size and risk score as independent prognostic factors significantly linked to patient outcomes (HR ≠ 1, $p < 0.05$; **Figure 6A**), and the PH assumption was validated ($p > 0.05$; **Table 1**). Multivariate Cox regression analysis further validated the risk score and tumor size as independent predictors of clinical prognosis (HR ≠ 1, $p < 0.05$; **Figure 6B**), with the PH assumption also met ($p > 0.05$; **Table 1**). A nomogram integrating the risk score and clinical features was developed to quantitatively predict patients' 3-, 5- and 7-year survival probabilities. As shown in **Figure 6C**, the total points derived from the sum of individual factor scores were applied to estimate survival probabilities of BC patients at 3-, 5- and 7-year. Higher total points indicated lower survival probability. The calibration curves indicate the nomogram's strong predictive accuracy (**Figure 6D**). Furthermore, the nomogram achieved AUC values exceeding 0.70 at 3-, 5- and 7-year (**Figure 6E**), demonstrating excellent predictive performance. This study established the clinical value of tumor size and risk score as independent prognostic factors for BC, and the developed nomogram provides a practical tool for individualized treatment decision-making, with potential to guide clinical practice.

Table 1 PH assumption test results

Varname	P
Univariate Cox regression analysis	
Riskscore	0.479
Age	0.205
ER status	0.285
Grade	0.446
Lymph node status	0.0157
Size	0.203
Multivariate Cox regression analysis	
Riskscore	0.475
Size	0.167

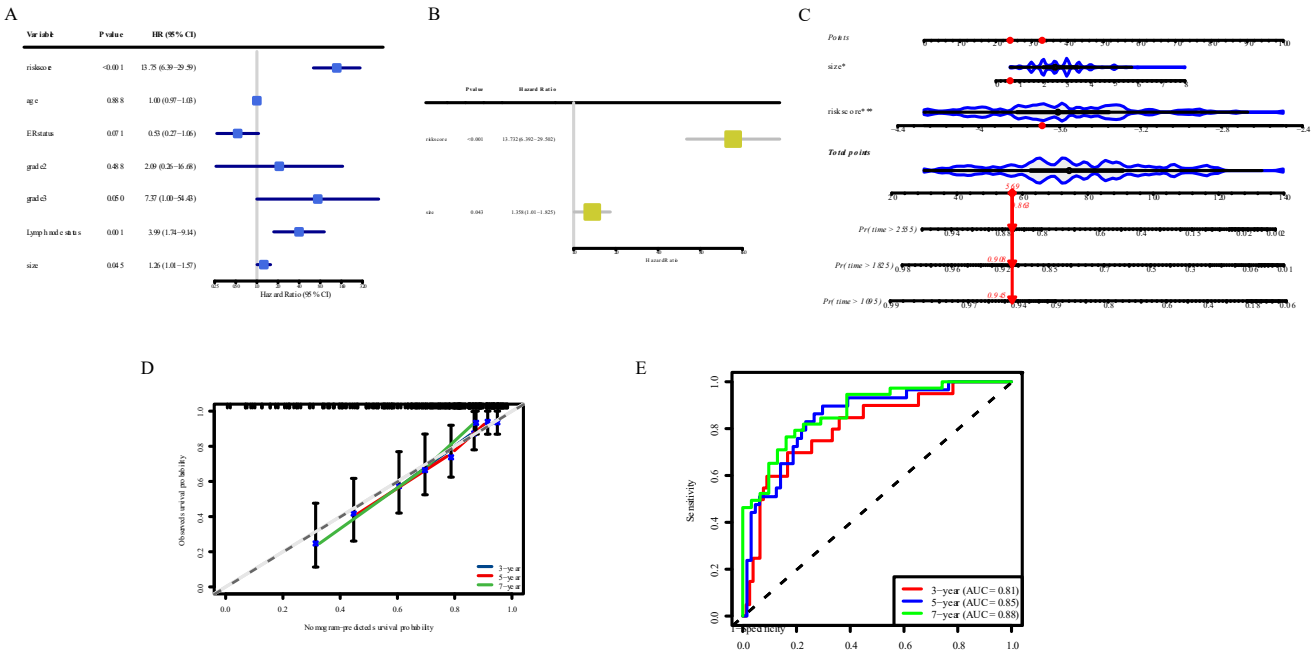


Fig. 6 Screening of independent prognostic factors and construction of the nomogram (A) Forest plot of univariable Cox regression analysis; (B) Forest plot of multivariable Cox regression analysis; (C) Nomogram; (D) Calibration curves; (E) ROC curves.

3.7 Risk stratification model reveals distinct immune microenvironment profiles and identifies core gene-immune cell interactions

Analysis of immune cell infiltration revealed that the risk model was closely related to the tumor immune microenvironment (**Figure 7A**). Infiltration levels of nine immune cell subtypes differed significantly between the HRG and LRG ($p < 0.05$) (**Figure 7B**). The HRG exhibited a distinct immune cell infiltration pattern, characterized by significantly elevated levels of seven cell types, including activated $CD4^+$T cells, $CD8^+$T cells, and CD56dim natural killer (NK)cells, while neutrophils and plasmacytoid dendritic cells demonstrated lower infiltration levels. Correlation network analysis revealed that these differentially-infiltrated immune cells had a complex cooperative regulation relationship **(Figure 7C)**. In particular, BNIP3L, KLHDC1 and PRDX3 were negatively correlated with MDSCs and activated CD4 T cells ($cor<-0.3$, $p<0.05$), of which KLHDC1 was also negatively correlated with activated CD8 T cells ($cor<-0.3$, $p<0.05$) **(Figure 7D)**. These results demonstrated a new mechanism by which the prognostic genes of TNBC regulate the tumor microenvironment by modulating immune cell infiltration, thus laying a theoretical foundation for combined approaches to immunotherapies.

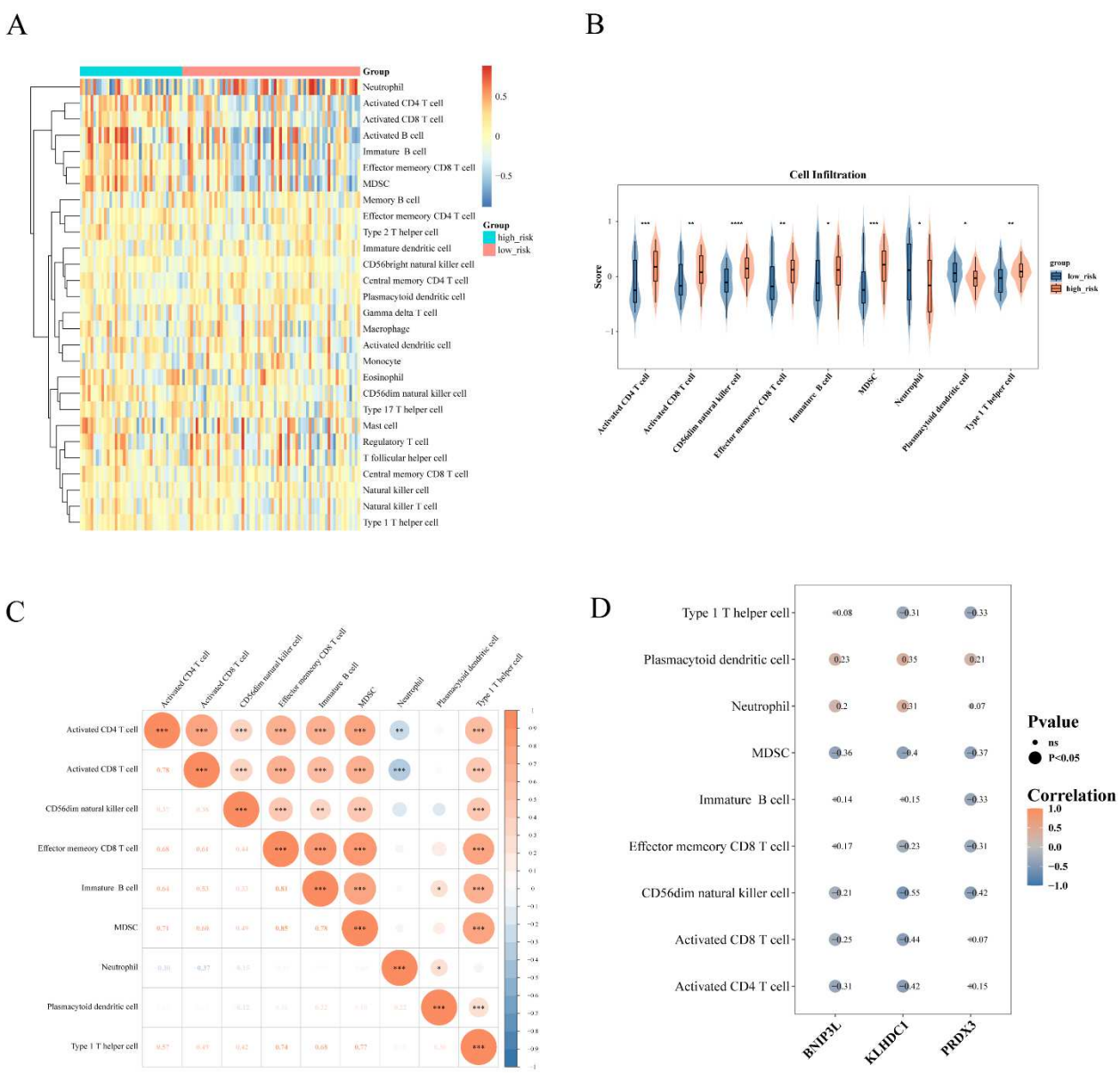


Fig. 7 Immune infiltration analysis in high-risk and low-risk groups (A) Abundance of infiltrating immune cells; (B) Differences in immune cell composition; (C) Correlations among differentially infiltrated immune cells; (D) Correlations between differentially infiltrated immune cells and prognostic genes. *p < 0.05, **p < 0.01, ***p < 0.001, ****p < 0.0001.

3.8 Differential immune checkpoint expression and metabolic reprogramming reveal dual mechanisms of tumor progression in risk-stratified BC

The expression of five immune checkpoint genes was detected to differ significantly between the HRG and LRG: LGALS9, CD86, CD200, CD44 and CD276 (**Figure 8A**). Significant relationships were observed between these immune checkpoint gene expression and the prognostic genes. Specifically, BNIP3L and KLHDC1 showed negative correlations with the expression of immunosuppressive genes LGALS9, CD86, and CD276 (cor< -0.3, p < 0.05), while demonstrating positive correlations with CD200 and CD44 (cor> 0.3, p < 0.05). PRDX3 exhibited a positive correlation with CD44 (cor> 0.3, p < 0.05) and a negative correlation with CD86 (cor< -0.3, p < 0.05) (**Figure 8B**). These correlation patterns provided new understanding of the molecular mechanisms underlying immune microenvironment dysregulation in high-risk BC.

GSEA revealed four significantly differentially enriched pathways (**Figure 8C**), including glycosphingolipid biosynthesis lactoand neolactoseries, xenobiotic metabolism mediated by cytochrome P450 enzymes, and catabolism of branched-chain amino acids, including leucine, valine, and isoleucine, which collectively delineated a coordinated network of metabolic reprogramming and microenvironmental adaptation in tumor progression.



Fig. 8 Immune checkpoint and GSEA in high-risk and low-risk groups (A) Differential expression of immune checkpoint genes; (B) Correlation heatmap; (C) GSEA for high-risk and low-risk groups. *p < 0.05, **p < 0.01, ***p < 0.001.

3.9 Drug sensitivity screening identifies 64 differential chemotherapeutic agents

Sensitivity screening of 251 chemotherapeutic drugs identified 64 agents with significant differential responses between the HRG and LRG (p < 0.05) (**Table S16**). Among these, the most promising drugs included BMS-509744, Gefitinib, LFM-A13, and AZD7762, which primarily belong to categories such as tyrosine kinase inhibitors and signaling pathway regulators (**Figure S1**). This study established a foundation for potential targeted therapies for high-risk patients and opened new avenues for understanding the mechanisms through which these genes influence therapeutic sensitivity.

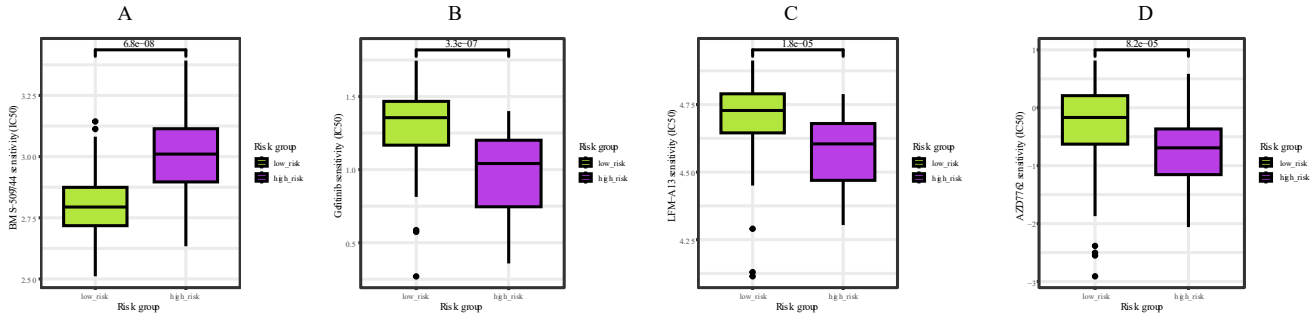


Fig. S1 Drug Sensitivity Analysis of High and Low-Risk Groups The top 4 chemotherapy drugs with the most significant differences between high and low-risk groups.(A) BMS-509744 sensitivity. (B) Gefitinib sensitivity. (C) LFM-A13 sensitivity. (D) AZD7762 sensitivity.

3.10 Expression levels of prognostic genes

As for RT-qPCR, the results revealed that BNIP3L and PRDX3 expression was significantly lower in BC samples than in the control group (p < 0.05), while KLHDC1 also exhibited reduced expression, but the difference was not found to be significant (p > 0.05) (**Figure 9**).

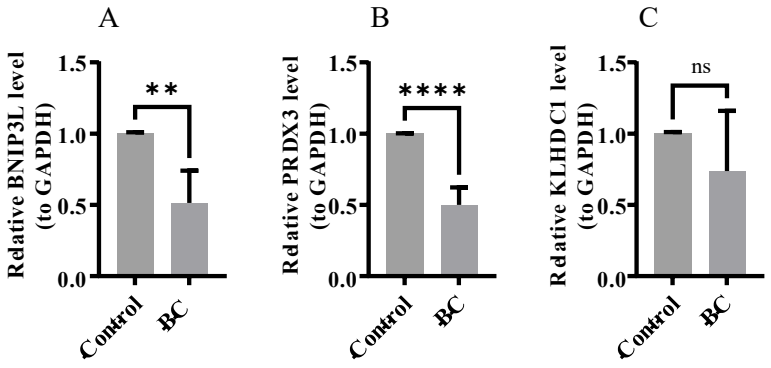


Fig. 9 Reverse transcription-polymerase chain reaction (RT-qPCR) results of prognostic gene (t-test) (A) BNIP3L expression. (B) PRDX3 expression. (C) KLHDC1 expression. * indicates $p < 0.05$; ** indicates $p < 0.01$; *** indicates $p < 0.001$; **** indicates $p < 0.0001$; ns indicates no significance.

4 Discussion

BC is a highly heterogeneous malignant tumor, its molecular subtypes closely related to treatment response and patient prognosis. Among them, TNBC has the worst prognosis due to a lack of therapeutic targets [35]. Research into unveiling new cell death mechanisms as potential therapeutic targets remains a high priority. This study aims to investigate the clinical relevance of triaptosis, a newly-defined oxidative cell death process, in BC. The core mechanism of triaptosis centers on pro-oxidant-induced mitochondrial ROS burst, which drives oxidation of PIK3C3 (VPS34 kinase), loss of PI (3)P, and subsequent endosomal dysfunction, ultimately triggering cell death [9]. We constructed a prognostic triaptosis-related model and identified three key genes—BNIP3L, KLHDC1, and PRDX3—as its core molecular regulators. These three genes collectively constitute a pathway network linking oxidative stress, metabolic reprogramming, and endosomal homeostasis, which converges on the regulation of triaptosis susceptibility in BC cells. It should be noted, however, that the evidence supporting each gene's direct role in BC tissue differs in strength. BNIP3L and PRDX3 were significantly validated at the tissue expression level, while KLHDC1 currently contributes robust prognostic signal at the bioinformatics level, with its tissue-level differential expression pending further confirmation. Their coordinated dysregulation not only explains malignant biological behavior, especially in treatment-resistant subtypes, but also provides an important theoretical basis for targeted therapy against triaptosis.

BNIP3L is a mitophagy receptor and a BCL-2 family protein located in the outer mitochondrial membrane. It directly binds to Autophagy-related protein 8 (Atg8) [36]. Previous studies in BC mainly showed that BNIP3L has a pro-apoptotic function. Targeted therapies against EGFR or HER2 could increase chemotherapy sensitivity by inducing BNIP3L expression through FoxO3a [37]. However, BNIP3L also plays a more complex role in BC. Under hypoxia, BNIP3L is induced by HIFs and triggers protective autophagy and mitophagy by dissociating the Bcl-2 – Beclin1 complex, thereby promoting tumor cell survival [38]. In TNBC, hypoxia-induced BNIP3L increases mitophagy and promotes cancer stem cell features, including self-renewal, CD44 expression, metabolic activity, and resistance to tamoxifen and palbociclib [39, 40]. These findings indicate that BNIP3L may regulate the mitochondrial source of ROS by controlling mitochondrial quality. During mitochondrial ROS bursts induced by menadione and other pro-oxidant agents, overexpression of BNIP3L may enhance the removal of damaged mitochondria through mitophagy. This may reduce oxidative stress and impede triaptosis-associated death. Thus, BNIP3L may connect mitochondrial quality control with triaptosis sensitivity.

PRDX3 (Peroxiredoxin 3) further strengthens this mitochondrial redox regulatory axis. PRDX3 is a mitochondria-specific antioxidant enzyme and is the most abundant and powerful scavenger of hydrogen peroxide in the mitochondrial matrix. It tends to self-oxidize and form inactive dimers to scavenge almost 90% of hydrogen peroxide in the mitochondrial matrix, thereby maintaining intracellular redox homeostasis [43-48]. PRDX3 has been reported to be closely associated with patient prognosis and may function as a protective biomarker [49]. However, PRDX3 can also regulate cancer cell survival through the B7-H4 pathway [50] and promote TNBC invasion and metastasis through the ERK-MMP-1 axis [51]. It is also involved in chemotherapy-induced skeletal muscle atrophy [52]. Under pro-oxidant-induced mitochondrial ROS burst, PRDX3 acts as a frontline antioxidant barrier. Functional deficiency of Peroxiredoxin 3 (PRDX3) may disturb ROS homeostasis, affect PI (3)P and endosomal function, and thereby regulate the occurrence of triaptosis. Therefore, BNIP3L and PRDX3 may cooperate at the mitochondrial level. BNIP3L reduces ROS leakage by removing damaged mitochondria, while PRDX3 clears hydrogen peroxide generated by oxidative phosphorylation.

Functional enrichment analysis further supports this link. Oxidative phosphorylation was highly enriched for BNIP3L and PRDX3. This suggests that these two genes are closely related to mitochondrial energy metabolism and redox homeostasis. Oxidative phosphorylation is the core function of mitochondria. It determines cellular ATP generation and also produces ROS as metabolic byproducts [53]. BNIP3L participates in mitochondrial quality control through selective removal of damaged or dysfunctional mitochondria. This directly influences oxidative phosphorylation efficiency, maintains the health of the mitochondrial pool, and reduces ROS leakage [54]. PRDX3 is the main hydrogen peroxide scavenger in mitochondria and constitutes the first line of antioxidant defense against ROS generated by oxidative phosphorylation [55]. Defective oxidative phosphorylation is a major source of intracellular ROS, and ROS burst is one of the core trigger factors for triaptosis [55]. Thus, oxidative phosphorylation provides a mechanistic bridge between BNIP3L, PRDX3, mitochondrial ROS homeostasis, and triaptosis.

Kelchdomain containing 1 (KLHDC1) may connect this mitochondrial redox axis with protein homeostasis and metabolic reprogramming. KLHDC1 is responsible for substrate recognition in the Cullin5-type E3 ubiquitin ligase complex through C-terminal glycine binding. It mediates the degradation of truncated SELENOS proteins induced by selenocysteine insertion defects, maintains redox homeostasis, and inhibits ER stress-induced cell death, suggesting a potential tumor-suppressive role [41, 42]. Although KLHDC1 has not been previously reported in breast carcinogenesis, we identified KLHDC1 for the first time as a prognostic biomarker in BC. Functional enrichment analysis showed that KLHDC1 was enriched in DNA replication and branched-chain amino acid degradation pathways, suggesting that it may coordinate proliferative demands with metabolic supply in cancer cells. Dysregulation of KLHDC1 may disturb protein homeostasis, induce ER stress, and disrupt ROS balance, thereby affecting cellular susceptibility to triaptosis. Since ROS burst and VPS34 oxidation are critical initiating events of triaptosis, KLHDC1 may regulate BC cell vulnerability to triaptosis by maintaining redox and metabolic homeostasis. This hypothesis provides a new perspective for understanding the tumor-suppressive effect of KLHDC1 and its role in triaptosis-related BC progression.

In summary, the three genes operate at distinct but complementary levels of this oxidative axis. BNIP3L controls mitochondrial quality and ROS output via mitophagy; PRDX3 directly scavenges mitochondrial hydrogen peroxide—both with tissue-level expression validation in BC. KLHDC1 may maintain protein and metabolic homeostasis to limit ROS accumulation, contributing a third regulatory layer supported by bioinformatics evidence. Taken together, their coordinated dysregulation is proposed to disrupt PI (3)P-dependent endosomal function and promote triaptosis in BC cells, though the direct tissue-level contribution of KLHDC1 warrants further experimental validation.

We further investigated the immune microenvironment alterations in BC through immune infiltration analysis. The high-risk group (HRG) exhibited a distinct immunometabolic microenvironment. It was characterized by increased numbers of activated $CD8^+$ T cells and CD56dim NK cells, but their functions were significantly inhibited. This may be closely related to metabolic reprogramming regulated by the three prognostic genes. Notably, all three prognostic genes showed significant negative correlations with MDSCs, collectively shaping the immunosuppressive microenvironment of BC.

MDSCs comprise a functionally and phenotypically diverse subset of immature myeloid cells expanded under pathological stress. They contribute to tumor immune evasion by fostering an immunosuppressive tumor microenvironment [56, 57]. The triaptosis axis—through dysregulation of mitochondrial ROS, metabolic reprogramming, and protein homeostasis—provides a mechanistic explanation for this negative correlation. BNIP3L may influence MDSC metabolism by regulating mitochondrial metabolic status, driving MDSCs to shift from glycolysis to oxidative phosphorylation to enhance their immunosuppressive function [58]. KLHDC1 may drive metabolic reorganization of tumor cells, leading to nutritional stress that enhances the suppressive function of MDSCs, though the precise mechanism remains to be clarified [42]. PRDX3 maintains oxidative metabolic homeostasis in tumor cells, which may support tumor cells in secreting specific cytokines or metabolites, thereby indirectly affecting the metabolic adaptation and functional maintenance of MDSCs [59, 60]. MDSCs with reshaped metabolic phenotypes then migrate to the tumor microenvironment, where they consume essential nutrients for immune cells by generating ROS and NO, inhibit the proliferation, differentiation, and cytotoxicity of T cells and NK cells, weaken the antigen-presenting capacity of B cells, and promote the recruitment and sustained activation of Tregs. This exacerbates local immune dysfunction and ultimately promotes immune escape and BC progression. Therefore, the oxidative stress – metabolic reprogramming axis driven by BNIP3L, KLHDC1, and PRDX3 synergistically shapes the immunosuppressive microenvironment of BC.

Drug sensitivity analysis further corroborates this triaptosis-centered axis. Out of 251 chemotherapeutic agents, 64 were identified with significantly diverse responses between the HRG and LRG ($p < 0.05$). Candidates such as BMS-509744, gefitinib, LFM-A13, and AZD7762 were primarily tyrosine kinases or signaling regulators. The HRG showed higher sensitivity to gefitinib, an EGFR inhibitor whose activity is not only associated with EGFR mutation status but also modulated by HER-specific ligand feedback regulation [61, 62]. BNIP3L, one of the resistance genes to tamoxifen and

palbociclib [40], is enriched in cell cycle-related pathways, allowing the inference that its altered expression in high-risk tumors may increase sensitivity to gefitinib by influencing HER ligand expression and trafficking. More broadly, all three prognostic genes regulate oxidative stress and metabolite homeostasis, suggesting that high-risk tumors harbor redox vulnerabilities. Since high-risk tumors are negatively correlated with MDSCs—immune cells that require ROS for suppressive activity—we speculate that metabolic remodeling by these three genes, through mitophagy, amino acid metabolism, and antioxidant modulatory mechanisms, establishes a scenario where EGFR inhibition disrupts compensatory metabolism and facilitates triaptosis induction. Thus, high-risk patients, despite having the worst prognosis, may exhibit more pronounced sensitivity to gefitinib: their metabolic status may be close to a tipping point where EGFR inhibition triggers oxidative damage and triaptosis. Collectively, these findings offer new insights into targeting high-risk BC and provide a new perspective for studying drug response through the prism of triaptosis.

To confirm the clinical significance of our bioinformatics findings, we conducted RT-qPCR to evaluate the three prognostic gene expression levels in clinical BC samples. The results provided partial but informative tissue-level support for the model. Both BNIP3L and PRDX3 were significantly downregulated in breast cancer tissues compared to adjacent normal tissues. This reduction in BNIP3L expression may impair mitophagy-dependent mitochondrial quality control, leading to accumulation of damaged mitochondria and excessive ROS production, thereby dynamically altering cellular sensitivity to triple-hit damage. Similarly, the notable decrease in PRDX3 levels may increase intracellular oxidative stress, disrupt oxidative balance, and promote the malignant development of BC cells. These findings directly corroborate their functional roles within the triaptosis axis at the tissue level.

However, KLHDC1 exhibited only a decreasing trend in BC tissues without reaching statistical significance. We acknowledge this as a meaningful limitation: the absence of significant differential expression in tissue samples weakens the direct evidence for KLHDC1 as a tissue-level biomarker or therapeutic target in BC. This discordance between bioinformatics-derived prognostic significance and tissue expression validation may reflect the relatively small clinical sample size, inherent tumor heterogeneity, or the possibility that KLHDC1 exerts its regulatory role through post-transcriptional mechanisms rather than transcriptional abundance alone.

Overall, the altered expression patterns of these three genes in clinical BC specimens support their pathogenic relevance and highlight their potential as critical components in triaptosis-related regulatory networks.

5 Conclusion

The role of triaptosisin BC prognosis was investigated through multi-omics analysis and three prognostic genes (BNIP3L, KLHDC1 and PRDX3) were identified to develop a highly effective predictive model. All these three genes are biologically related to triaptosisregulation. However, it must be pointed out that our study is solely based on retrospective bioinformatic analysis, we could not verify the precise mechanisms of the above genes in triaptosis. In the following investigations, in vitro and in vivo experimental models are necessary to determine their functions, especially in oxidative stress and metabolic reprogramming, and thus promote the clinical translational application of triaptosis-related biomarkers.

6 Declarations

6.1 Data availability statement

The dataset GSE42568 can from the Gene Expression Omnibus (GEO) database (https://www.ncbi.nlm.nih.gov/geo/query/acc.cgi?acc=GSE42568) (sequencing platform: GPL570; sequencing type: array; download date: 2025-09-20). The dataset GSE20685 can downloaded from the GEO database (https://www.ncbi.nlm.nih.gov/geo/query/acc.cgi?acc=GSE20685) (sequencing platform: GPL570; sequencing type: array; download date: 2025-09-20). The code used in this article is available at the Github (URL: https://github.com/selpink808/my-R-code/releases/tag/v1.0.0) provided. The original contributions presented in the study are included in the article and supplementary material. Further enquiries can be directed to the corresponding authors.

6.2 Ethical Approval and Accordance

This study was approved by the Ethics Committee of Shenzhen Second People's Hospital (Approval Number: 2026-006-02PJ). All procedures performed in studies involving human participants were in accordance with the ethical standards of the institutional and/or national research committee and with the 1964 Helsinki Declaration and its later amendments or comparable ethical standards.

6.3 Consent to participate

Informed consent was obtained from all individual participants included in the study.

6.4 Consent to publish

Informed consent for publication of the study data was obtained from all participants.

6.5 Funding sources

This research did not receive any specific grant from funding agencies in the public, commercial, or not-for-profit sectors.

6.6 Conflict of Interest

The authors declare that they have no known competing financial interests or personal relationships that could have appeared to influence the work reported in this paper.

References

1. Harbeck N, Penault-Llorca F, Cortes J, Gnant M, Houssami N, Poortmans P et al. Breast cancer. Nature reviews. Disease primers. (2019) 5. doi: 10.1038/s41572-019-0111-2

2. Loibl S, Poortmans P, Morrow M, Denkert C, Curigliano G. Breast cancer. Lancet (London, England). (2021) 397. doi: 10.1016/S0140-6736(20)32381-3

3. Wagle Ns, Nogueira L, Devasia Tp, Mariotto Ab, Yabroff Kr, Islami F et al. Cancer treatment and survivorship statistics, 2025. CA: a cancer journal for clinicians. (2025) 75. doi: 10.3322/caac.70011

4. Shafei Ma, Flemban A, Daly C, Kendrick P, White P, Dean S et al. Differential expression of the BCAT isoforms between breast cancer subtypes. Breast cancer (Tokyo, Japan). (2021) 28. doi: 10.1007/s12282-020-01197-7

5. Li Y, Zhang H, Merkher Y, Chen L, Liu N, Leonov S et al. Recent advances in therapeutic strategies for triple-negative breast cancer. Journal of hematology & oncology. (2022) 15. doi: 10.1186/s13045-022-01341-0

6. Katsura C, Ogunmwonyi I, Kankam Hk, Saha S. Breast cancer: presentation, investigation and management. British journal of hospital medicine (London, England : 2005). (2022) 83. doi: 10.12968/hmed.2021.0459

7. Khan Mm, Yalamarty Ssk, Rajmalani Ba, Filipczak N, Torchilin Vp. Recent strategies to overcome breast cancer resistance. Critical reviews in oncology/hematology. (2024) 197. doi: 10.1016/j.critrevonc.2024.104351

8. Liu J, Hong M, Li Y, Chen D, Wu Y, Hu Y. Programmed Cell Death Tunes Tumor Immunity. Frontiers in immunology. (2022) 13. doi: 10.3389/fimmu.2022.847345

9. Li Zz, Zhou K, Wu J, Cao Lm, Wang Gr, Luo Hy et al. Triaptosis and Cancer: Next Hope?. Research (Washington, D.C.). (2025) 8. doi: 10.34133/research.0880

10. Tang D, Kang R, Kroemer G. Triaptosis: an endosome-dependent cell death modality. Cell research. (2025) 35. doi: 10.1038/s41422-024-01053-9

11. Swamynathan Mm, Kuang S, Watrud Ke, Doherty Mr, Gineste C, Mathew G et al. Dietary pro-oxidant therapy by a vitamin K precursor targets PI 3-kinase VPS34 function. Science (New York, N.Y.). (2024) 386. doi: 10.1126/science.adk9167

12. Clarke C, Madden Sf, Doolan P, Aherne St, Joyce H, O'driscoll L et al. Correlating transcriptional networks to breast cancer survival: a large-scale coexpression analysis. Carcinogenesis. (2013) 34. doi: 10.1093/carcin/bgt208

13. Kao Kj, Chang Km, Hsu Hc, Huang At. Correlation of microarray-based breast cancer molecular subtypes and clinical outcomes: implications for treatment optimization. BMC cancer. (2011) 11. doi: 10.1186/1471-2407-11-143

14. Xie J, Zhang M, Qi M. Integrating Machine Learning Algorithms to Construct a Triaptosis-Related Prognostic Model in Melanoma. Cancer management and research. (2025) 17. doi: 10.2147/CMAR.S525738

15. Hänzelmann S, Castelo R, Guinney J. GSVA: gene set variation analysis for microarray and RNA-seq data. BMC bioinformatics. (2013) 14. doi: 10.1186/1471-2105-14-7

16. Shi Y, Wang Y, Dong H, Niu K, Zhang W, Feng K et al. Crosstalk of ferroptosis regulators and tumor immunity in pancreatic adenocarcinoma: novel perspective to mRNA vaccines and personalized immunotherapy. Apoptosis : an international journal on programmed cell death. (2023) 28. doi: 10.1007/s10495-023-01868-8

17. Deng X, Thompson Ja. An R package for Survival-based Gene Set Enrichment Analysis. Research square. (2023) doi: 10.21203/rs.3.rs-3367968/v1

18. Wu T, Hu E, Xu S, Chen M, Guo P, Dai Z et al. clusterProfiler 4.0: A universal enrichment tool for interpreting omics data. Innovation (Cambridge (Mass.)). (2021) 2. doi: 10.1016/j.xinn.2021.100141

19. Love Mi, Huber W, Anders S. Moderated estimation of fold change and dispersion for RNA-seq data with DESeq2. Genome biology. (2014) 15. doi: 10.1186/s13059-014-0550-8

20. Ito K, Murphy D. Application of ggplot2 to Pharmacometric Graphics. CPT: pharmacometrics & systems pharmacology. (2013) 2. doi: 10.1038/psp.2013.56

21. Gu Z, Eils R, Schlesner M. Complex heatmaps reveal patterns and correlations in multidimensional genomic data. Bioinformatics (Oxford, England). (2016) 32. doi: 10.1093/bioinformatics/btw313

22. Gao Ch, Chen C, Akyol T, Dusa A, Yu G, Cao B et al. ggVennDiagram: Intuitive Venn diagram software extended. iMeta. (2024) 3. doi: 10.1002/imt2.177

23. Marier Jf, Teuscher N, Mouksassi Ms. Evaluation of covariate effects using forest plots and introduction to the coveffectsplot R package. CPT: pharmacometrics & systems pharmacology. (2022) 11. doi: 10.1002/psp4.12829

24. Engebretsen S, Bohlin J. Statistical predictions with glmnet. Clinical epigenetics. (2019) 11. doi: 10.1186/s13148-019-0730-1

25. Liberzon A, Birger C, Thorvaldsdóttir H, Ghandi M, Mesirov Jp, Tamayo P. The Molecular Signatures Database (MSigDB) hallmark gene set collection. Cell systems. (2015) 1. doi: 10.1016/j.cels.2015.12.004

26. Orifjon S, Jammatov J, Sousa C, Barros R, Vasconcelos O, Rodrigues P. Translation and Adaptation of the Adult Developmental Coordination Disorder/Dyspraxia Checklist (ADC) into Asian Uzbekistan. Sports (Basel, Switzerland). (07/17/2023) 11. doi: 10.3390/sports11070135

27. Shannon P, Markiel A, Ozier O, Baliga Ns, Wang Jt, Ramage D et al. Cytoscape: a software environment for integrated models of biomolecular interaction networks. Genome research. (2003 Nov) 13. doi: 10.1101/gr.1239303

28. Huang S, Lai H, Pan X, Lin Q, Qin Y, Liu F et al. Development and Validation of a Nomogram for Predicting Survival Based on Ferritin and Transferrin Ratio in Breast Cancer Patients. Cancer control : journal of the Moffitt Cancer Center. (2024) 31. doi: 10.1177/10732748241261553

29. Xu S, Qiu L, Xu L, Liu Y, Zhang J. Development and validation of a nomogram for assessing hepatocellular carcinoma risk after SVR in hepatitis C patients with advanced fibrosis and cirrhosis. Infectious agents and cancer. (2024) 19. doi: 10.1186/s13027-024-00578-3

30. Blanche P, Dartigues Jf, Jacqmin-Gadda H. Estimating and comparing time-dependent areas under receiver operating characteristic curves for censored event times with competing risks. Statistics in medicine. (2013) 32. doi: 10.1002/sim.5958

31. Zhang Z, Kattan Mw. Drawing Nomograms with R: applications to categorical outcome and survival data. Annals of translational medicine. (2017 May) 5. doi: 10.21037/atm.2017.04.01

32. Wang L, Wang D, Yang L, Zeng X, Zhang Q, Liu G et al. Cuproptosis related genes associated with Jab1 shapes tumor microenvironment and pharmacological profile in nasopharyngeal carcinoma. Frontiers in immunology. (2022) 13. doi: 10.3389/fimmu.2022.989286

33. Xue C, Gu X, Zhao Y, Jia J, Zheng Q, Su Y et al. Prediction of hepatocellular carcinoma prognosis and immunotherapeutic effects based on tryptophan metabolism-related genes. Cancer cell international. (2022) 22. doi: 10.1186/s12935-022-02730-8

34. Geeleher P, Cox N, Huang Rs. pRRophetic: an R package for prediction of clinical chemotherapeutic response from tumor gene expression levels. PloS one. (2014) 9. doi: 10.1371/journal.pone.0107468

35. A. Szymiczek, A. Lone, M. R. Akbari. Molecular intrinsic versus clinical subtyping in breast cancer: A comprehensive review. Clin Genet. (2021) 99, 613-637. doi: 10.1111/cge.13900

36. Novak I, Kirkin V, Mcewan Dg, Zhang J, Wild P, Rozenknop A et al. Nix is a selective autophagy receptor for mitochondrial clearance. EMBO reports. (2010) 11. doi: 10.1038/embor.2009.256

37. Real Pj, Benito A, Cuevas J, Berciano Mt, De Juan A, Coffer P et al. Blockade of epidermal growth factor receptors chemosensitizes breast cancer cells through up-regulation of Bnip3L. Cancer research. (2005) 65. doi: 10.1158/0008-5472.CAN-05-1134

38. Bellot G, Garcia-Medina R, Gounon P, Chiche J, Roux D, Pouysségur J et al. Hypoxia-induced autophagy is mediated through hypoxia-inducible factor induction of BNIP3 and BNIP3L via their BH3 domains. Molecular and cellular biology. (2009) 29. doi: 10.1128/MCB.00166-09

39. Liu Y, Zhang H, Liu Y, Zhang S, Su P, Wang L et al. Hypoxia-induced GPCPD1 depalmitoylation triggers mitophagy via regulating PRKN-mediated ubiquitination of VDAC1. Autophagy. (2023) 19. doi: 10.1080/15548627.2023.2182482

40. Mauro-Lizcano M, Sotgia F, Lisanti Mp. Mitophagy and cancer: role of BNIP3/BNIP3L as energetic drivers of stemness features, ATP production, proliferation, and cell migration. Aging. (2024) 16. doi: 10.18632/aging.205939

41. Chin Kt, Xu Ht, Ching Yp, Jin Dy. Differential subcellular localization and activity of kelch repeat proteins KLHDC1 and KLHDC2. Molecular and cellular biochemistry. (2007) 296. doi: 10.1007/s11010-006-9304-6

42. Okumura F, Fujiki Y, Oki N, Osaki K, Nishikimi A, Fukui Y et al. Cul5-type Ubiquitin Ligase KLHDC1 Contributes to the Elimination of Truncated SELENOS Produced by Failed UGA/Sec Decoding. iScience. (2020) 23. doi: 10.1016/j.isci.2020.100970

43. Wang Z, Sun R, Wang G, Chen Z, Li Y, Zhao Y et al. SIRT3-mediated deacetylation of PRDX3 alleviates mitochondrial oxidative damage and apoptosis induced by intestinal ischemia/reperfusion injury. Redox biology. (2020) 28. doi: 10.1016/j.redox.2019.101343

44. Kang Sw, Chae Hz, Seo Ms, Kim K, Baines Ic, Rhee Sg. Mammalian peroxiredoxin isoforms can reduce hydrogen peroxide generated in response to growth factors and tumor necrosis factor-alpha. The Journal of biological chemistry. (1998) 273. doi: 10.1074/jbc.273.11.6297

45. Cox Ag, Winterbourn Cc, Hampton Mb. Mitochondrial peroxiredoxin involvement in antioxidant defence and redox signalling. The Biochemical journal. (2009) 425. doi: 10.1042/BJ20091541

46. Cadenas E. Mitochondrial free radical production and cell signaling. Molecular aspects of medicine. (2004) 25. doi: 10.1016/j.mam.2004.02.005

47. Brown Kk, Eriksson Se, Arnér Es, Hampton Mb. Mitochondrial peroxiredoxin 3 is rapidly oxidized in cells treated with isothiocyanates . Free radical biology & medicine. (2008) 45. doi: 10.1016/j.freeradbiomed.2008.04.030

48. Peskin Av, Low Fm, Paton Ln, Maghzal Gj, Hampton Mb, Winterbourn Cc. The high reactivity of peroxiredoxin 2 with H(2)O(2) is not reflected in its reaction with other oxidants and thiol reagents. The Journal of biological chemistry. (2007) 282. doi: 10.1074/jbc.M700339200

49. Mei J, Hao L, Liu X, Sun G, Xu R, Wang H et al. Comprehensive analysis of peroxiredoxins expression profiles and prognostic values in breast cancer. Biomarker research. (08/06/2019) 7. doi: 10.1186/s40364-019-0168-9

50. Chen Hc, Long M, Gao Zw, Liu C, Wu Xn, Yang L et al. Silencing of B7-H4 induces intracellular oxidative stress and inhibits cell viability of breast cancer cells via downregulating PRDX3. Neoplasma. (2022) 69. doi: 10.4149/neo_2022_220304N241

51. Chua Pj, Ow Sh, Ng Ct, Huang Wh, Low Jt, Tan Ph et al. Peroxiredoxin 3 regulates breast cancer progression via ERK-mediated MMP-1 expression. Cancer cell international. (02/06/2024) 24. doi: 10.1186/s12935-024-03248-x

52. Guigni Ba, Callahan Dm, Tourville Tw, Miller Ms, Fiske B, Voigt T et al. Skeletal muscle atrophy and dysfunction in breast cancer patients: role for chemotherapy-derived oxidant stress. American journal of physiology. Cell physiology. (2018) 315. doi: 10.1152/ajpcell.00002.2018

53. Nsiah-Sefaa A, Mckenzie M. Combined defects in oxidative phosphorylation and fatty acid β-oxidation in mitochondrial disease. Bioscience reports. (2016) 36. doi: 10.1042/BSR20150295

54. Townley Ar, Wheatley Sp. Mitochondrial survivin reduces oxidative phosphorylation in cancer cells by inhibiting mitophagy. Journal of cell science. (2020) 133. doi: 10.1242/jcs.247379

55. Lee H, Kim Bw, Lee Jw, Hong J, Lee Jw, Kim Hl et al. Extracellular reactive oxygen species are generated by a plasma membrane oxidative phosphorylation system. Free radical biology & medicine. (2017) 112 doi: 10.1016/j.freeradbiomed.2017.08.016

56. Sanchez-Pino Md, Dean Mj, Ochoa Ac. Myeloid-derived suppressor cells (MDSC): When good intentions go awry. Cellular immunology. (2021) 362. doi: 10.1016/j.cellimm.2021.104302

57. Salminen A, Kauppinen A, Kaarniranta K. AMPK activation inhibits the functions of myeloid-derived suppressor cells (MDSC): impact on cancer and aging. Journal of molecular medicine (Berlin, Germany). (2019) 97. doi: 10.1007/s00109-019-01795-9

58. Han X, Song X, Xiao Z, Zhu G, Gao R, Ni B et al. Study on the mechanism of MDSC-platelets and their role in the breast cancer microenvironment. Frontiers in cell and developmental biology. (2024) 12. doi: 10.3389/fcell.2024.1310442

59. T. Abimannan, D. Peroumal, J. R. Parida, P. K. Barik, P. Padhan, S. Devadas. Oxidative stress modulates the cytokine response of differentiated Th17 and Th1 cells. Free Radic Biol Med. (2016) 99, 352-363. doi: 10.1016/j.freeradbiomed.2016.08.026

60. R. Li, M. B. Mukherjee, J. Lin. Coordinated Regulation of Myeloid-Derived Suppressor Cells by Cytokines and Chemokines. Cancers (Basel). (2022) 14. doi: 10.3390/cancers14051236

61. A. El Guerrab, M. Bamdad, Y. J. Bignon, F. Penault-Llorca, C. Aubel. Co-targeting EGFR and mTOR with gefitinib and everolimus in triple-negative breast cancer cells. Sci Rep. (2020) 10, 6367. doi: 10.1038/s41598-020-63310-2

62. L. Ferrer-Soler, A. Vazquez-Martin, J. Brunet, J. A. Menendez, R. De Llorens, R. Colomer. An update of the mechanisms of resistance to EGFR-tyrosine kinase inhibitors in breast cancer: Gefitinib (Iressa) -induced changes in the expression and nucleo-cytoplasmic trafficking of HER-ligands (Review). Int J Mol Med. (2007) 20, 3-10.

Supplementary Files

This is a list of supplementary files associated with this preprint. Click to download.

- TableS.zip
- FigureS.zip